Electronic Supplementary Material (ESI) for Journal of Materials Chemistry B.

SUPPORTING INFORMATION

Laser-induced zinc oxide/graphene photoelectrode toward photocurrent-polarity-switching photoelectrochemical biosensor with bipedal DNA walker amplification

Zhenli Qiu,[a,c] Yufen Lei,[a,c] Xintong Lin,[a,c] Jinman Zhu,[a,c] Ruijin Zeng,[b] Rongjian Sa,[a] Dianping Tang,[b] Qiang Chen[a,*], Yiting Chen[a,c,*]

[a]*Fujian Provincial University Engineering Research Center of Green Materials and Chemical Engineering, College of Materials and Chemical Engineering, Minjiang University, Fuzhou 350108, PR China.* [b]*Key Laboratory of Analysis and Detection for Food Safety (MOE & Fujian Province), State Key Laboratory of Photocatalysis on Energy and Environment, Department of Chemistry, Fuzhou University, Fuzhou 350108, China.*

[c]*College of Environment & Safety Engineering, Fuzhou University, Fuzhou, 350108, PR China*

∗ *Corresponding author.*

E-mail:jocq8@mju.edu.cn; cyt@mju.edu.cn

TABLE OF CONTENTS

EXPERIMENTAL SECTION

Reagents and materials. The reagents and materials used in this experiment included mainly zinc chloride ($ZnCl_2$, AR), polyacrylic acid (PAA, AR), hemin chloride (hemin, AR), 6-mercapto-1-hexanol (MCH, AR), which was purchased from Shanghai Aladdin Biochemical Technology Co. N,N-dimethylformamide (DMF, AR), chloroauric acid ($HAuCl_4$-$4H_2O$, AR), and potassium nitrate (KNO_3, AR) were purchased from Sinopharm Chemical Reagent Co. The oligonucleotide sequences used in the experiments are listed in Table S1. All oligonucleotides, nucleic acid exonuclease III (Exo III), phosphate buffered saline (PBS Buffer, 5×, pH 7.2-7.4), tobramycin (TOB), gentamicin sulfate (GES), ciprofloxacin hydrochloride (CIH), oxytetracycline hydrochloride (OXH), chloramphenicol hydrochloride (CAP), kanamycin sulfate(KAS), ampicillin sodium(AMS) were bought from Shanghai Bioengineering Co. The ultrapure water used during the experiments was provided by an ultrapure water machine (Direct-Q, Millipore Corporation, USA). Before the experiment, the C1/C2/A-DNA complex formed by mixing C1, C2 and A-DNA, as well as other oligonucleotides, was kept at 95 °C for 5 min and then naturally cooled to indoor temperature.

Table S1. Oligonucleotide sequences used in this study.

Oligonucleotide name	Sequence (5' to 3') description
Hairpin probe 1(HP1)	GGGACTTGGTTTAGGTAATGAGTCCCCCTAAACCAAGTCCCTAGCCC
Hairpin probe 2 (HP2)	*AAGTCCCTAGCCCTTTATCACTATCTTTCTCACACACAAGTCCCTAGCCC*TAGTGA TAAAGGGCTAGGGACTTGGTTTAGG
C1	GTCATTCAATCAAGGTGTGCATCTTTC
C2	CGATCGAAGTCCCATTC
A-DNA	GGGCTAGGGACTTCGATCGGATGCACACCTTGATTGAATGACATATAT-SH
G-DNA	AGGGTGGGGAGGGTGGGGGTCATTCAATCAAGGTGTGCTCCGATCGAAGTCC CTAGTTT

The underlined HP1 sequence in this work is the aptamer of tobramycin, and the italicized HP2 sequence is BW.

Apparatus and measurements. Field emission scanning electron microscope (SU8000, Hitachi,

Japan); Transmission electron microscope (Talos F200X, FEI, USA); Zeta potential and nanoparticle size analyzer (Zetasizer Nano ZS90, Malvern); X-ray scanner (Minifelx, RIKEN, Japan); Raman spectrometer (DXR2, Thermo); X-ray photoelectron spectrum analyzer (Verios G 4UC, Thermo Fisher Scientific); Nano-laser action instrument (Laser Nano Pro, Tianjin Jiayin Nanotechnology Co., Ltd.); Vertical electrophoresis tank (DYC-Mini4, Nanjing Yucheng Experimental Equipment Co.); Gel electrophoresis instrument (DYY-600E, Beijing Dongfang Ruili Electrophoresis Equipment Co., Ltd.). Photoelectrochemical measurements (i-t) and cyclic voltammetry (CV) were performed using an electrochemical workstation (CHI-760D, Shanghai Chenhua Instruments Co., Ltd.) combined with a conventional three-electrode system, using Ag/AgCl or saturated glycerol electrodes as reference electrodes, platinum wire electrodes as auxiliary electrodes, and modified ITO electrodes as working electrodes. I-t was performed in a 0.1 M Na_2SO_4 solution. CV was performed in a gold deposition solution containing 0.1 M KNO_3 and 2 mM $HAuCl_4$.

Preparation of the ZnO/LIG/ITO electrode. According to the laser direct writing method reported in the literature.[1] In this study, ZnO/LIG modified ITO electrodes were prepared. First, $ZnCl_2$ powder and PAA powder were dissolved in DMF in a certain weight ratio and stirred continuously at room temperature overnight to thoroughly mix in the atmosphere to obtain a viscous and homogeneous PAA mixture containing Zn^{2+} (Zn^{2+}-PAA precursor). The Zn^{2+}-PAA precursors were placed under vacuum until the tiny air bubbles were removed. The ITO glass was then ultrasonically cleaned using ethanol and ultrapure water in turn for 30 min, and after rinsing with a large amount of ultrapure water, clean ITO glass was obtained by natural drying. The Zn^{2+}-PAA precursor was suspended uniformly on the ITO glass surface using a coater at 1000 r·min^{-1} for 60 s (suspension area 1 cm × 1 cm). The ITO electrode loaded with Zn^{2+}-PAA precursors on the surface was placed in an oven at 180 °C and dried for 30 min to form a Zn^{2+} co-doped PAA film. After natural cooling, the pre-designed patterns were scribed onto the Zn^{2+} co-doped PAA films using a computer-controlled nanolaser action instrument to generate the ZnO/LIG/ITO electrodes in situ.

Treatment and modification of the Au/ZnO/LIG/ITO electrodes. The electrodeposition method according to the literature reported.[2] Au/ZnO/LIG/ITO electrodes were prepared on this basis. Kapton polyimide tape was applied to the ZnO/LIG/ITO electrode to avoid contact between the electrolyte and the conductive part during the test, and the three-electrode system was combined with the CV method and scanned at a scan rate of 50 mV/s from -0.9 V to -0.1 V for 30 consecutive cycles in a solution containing 0.1 M KNO_3 and 2 mM $HAuCl_4$. The resulting Au/ZnO/LIG/ITO electrodes were washed with ultrapure water and dried at room temperature prior to use. Next, the Au/ZnO/LIG/ITO electrode was modified with oligonucleotides. 12 μL of C1/C2/A-DNA (2 μM) mixture was dropped onto Au/ZnO/LIG/ITO electrodes and incubated at 37 ° C for 2 h. DNA was bound to the electrodes by gold thiol bonds. These electrodes were rinsed with PBS (10 mM, pH 7.4) to remove oligonucleotide chains that were not adsorbed.

Subsequently, to avoid nonspecific adsorption effects, these electrodes were immersed in a 2 mM solution of 6-mercapto-l-hexanol (MCH) for 1 h to close the unoccupied electrode sites. The C1/C2/A-DNA/Au/ZnO/LIG/ITO electrodes were rinsed again with PBS (10 mM, pH 7.4) and dried at room temperature, and the photocurrents were detected using the i-t method in a solution of 0.1 M Na_2SO_4, and the test values were the photocurrent values of the original electrodes.

DFT calculation details. Our density functional theory (DFT) calculations were carried out to obtain the band position for crystal materials and energy levels for Hemin molecule.[3,4] The Vienna ab initio simulation package (VASP) based on the plane-wave basis sets with the projector augmented-wave method was used to calculate the band structure of Au (111) surface, graphene and bulk ZnO.[5,6] The HOMO and LUMO position for Hemin molecule was calculated with Gaussian 16 package. The hybrid functional PBE0 was used to treat the exchange-correlation potential in the both two packages.[7,8] The structures of Au (111) surface, graphene and bulk ZnO were optimized with a generalized gradient approximation (GGA) with the Perdew-Burke-Ernzerhof (PBE) parametrization.[9] The van der Waals correction of Grimme's DFT-D3 model was also adopted.[10] The energy cutoff was set to be 600 eV. The structures were fully relaxed until the maximum force on each atom was less than 0.01 eV/Å, and the energy convergent standard was 10^{-7} eV. The Brillouin-zone integration was sampled with a Γ-centered Monkhorst-Pack mesh of 21 × 21 × 1 for Au (111) surface, 24 × 24 × 1 for graphene and 21 × 21 × 10 for bulk ZnO.[11] In hybrid functional calculation, the Brillouin-zone integration was sampled with a Γ-centered Monkhorst-Pack mesh of 12 × 12 × 1 for Au (111) surface, 18 × 18 × 1 for graphene and 12 × 12 × 5 for bulk ZnO.[11] The work function for Au (111) surface and graphene was also calculated to align the position of Fermi energy level to the same vacuum level as zero. The CB position for ZnO was from the published work.[12] The structures for Hemin molecules with different spin multiplicity (2S+1) values of 2, 4, and 6 were compared to determine the most stable structure. The structures were optimized with PBE0/def2-SVP level.[7,8,13] The free energy and the energy levels were also derived at this level.

Polypropylene gel electrophoresis(PAGE). The DNA (2 uL) was thoroughly mixed with loading buffer (1 uL), and this mixed sample was upsampled into a 12% polyacrylamide gel. Electrophoresis was carried out in an electrophoresis tank with 1×TBE as electrolyte, and the electrophoresis apparatus was set to 200 V for 45 min. After electrophoresis, the gel was stained with 4S Red Plus in a thermostatic oscillator protected from light for 90 min. finally, the gel could be photographed and recorded by a fully automated gel imaging system.

PARTIAL RESULTS

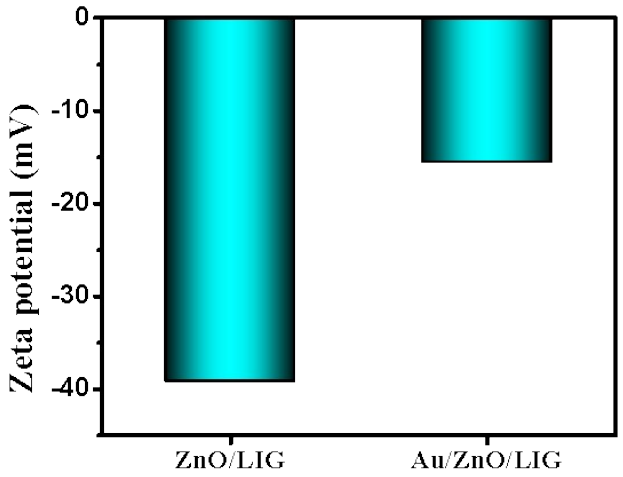

Fig S1. Zeta potential of ZnO/LIG and Au/ZnO/LIG.

Optimization of experimental conditions

The performance of the sensor is related to several factors and, based on the above experimental design, seven of the most important parameters were selected for optimization, including the mass ratio of PAA to $ZnCl_2$, LDW power, gold deposition cycle, Exo III concentration, DNA walker reaction time, hemin concentration and incubation time of hemin and G-quadruplex.

The photocurrent response increases as the mass ratio of PAA to $ZnCl_2$ increases, and the photocurrent reaches a maximum value when the mass ratio is 1:1 (Fig. S2A). Furthermore, the photocurrent decreases when the mass ratio exceeds 1:1. This may be attributed to the generation of electron-hole pairs by the ZnO induced by lasers under visible-light irradiation, which passes through graphene to the electrode surface and generates photocurrents. Therefore, the doping amount of PAA as a graphene precursor affects the electron transfer efficiency on the electrode surface. An appropriate mass of PAA can activate the advantages of graphene, and the porous structure is favorable for wrapping ZnO NPs. This endows the electrode material with good photoelectric activity, whereas an excessive amount of PAA adversely affects photoelectric performance. On the basis of the above results, the mass ratio of PAA to $ZnCl_2$ was selected as 1:1 for subsequent experiments.

Fig. S2B shows the relation between the LDW power and the photocurrent response. The strongest value of the photocurrent signal is obtained when the laser power is 10 W. A considerably small laser power is insufficient to completely generate ZnO/LIG from the Zn^{2+}-PAA film on the surface of ITO glass,

whereas a considerably large laser power causes excessive carbonization of graphene, damaging the electrode surface and affecting the electrode conductivity. Therefore, the optimal laser power for electrode preparation is 10 W. More Au NPs are loaded on the surface with a longer gold deposition cycle of the electrode, which affects the photocurrent response of the electrode. As shown in Fig. S2C, the maximum photocurrent occurs when the gold deposition period is 30. Considerably high or low concentrations of Au NPs adversely affect the electrode; thus, 30 cycles were chosen as the optimal value for gold deposition in subsequent experiments.

Fig. S2D examines the effect of Exo III concentration on the absolute value of the photocurrent flip-flop. The photocurrent response increases with increasing Exo III concentration until a plateau is reached at 10 U. Therefore, the Exo III concentration was selected to be 10 U in subsequent experiments. Fig. S2E depicts the relation between the DNA walker incubation time and the photocurrent response. The time of DNA incubation on the electrode plays a crucial role in the efficiency of the DNA walker reaction. The photocurrent response tends to plateau when the incubation time is 2 h, indicating that 2 h can make the DNA walker reaction sufficient. Therefore, the DNA walker reaction time was selected as 2 h for subsequent experiments.

In addition, because the G-quadruplex could trap hemin onto the electrode surface and form a hemin/G-quadruplex complex, the combined effect with ZnO/LIG caused a photocurrent polarity flip phenomenon from anodic to cathodic photocurrents. Therefore, the concentration of hemin and the binding time of hemin and G-quadruplex are critical for the current response of the biosensor. Fig. S2F shows that the photocurrent response becomes stronger with higher hemin concentration. The photocurrent variation tends to be smooth when the hemin concentration is greater than 200 mM. Therefore, a hemin concentration of 200 mM was subsequently selected for the experiment. As shown in Fig. S2G, more hemin binds to the G-quadruplex with increasing time. When the binding time was 60 min, the absolute value of photocurrent reversed to a maximum and then stabilized, indicating that 60 min was sufficient to form hemin/G-quadruplex complexes. Therefore, 60 min was taken as the optimal binding time for hemin and the G-quadruplex in subsequent experiments.

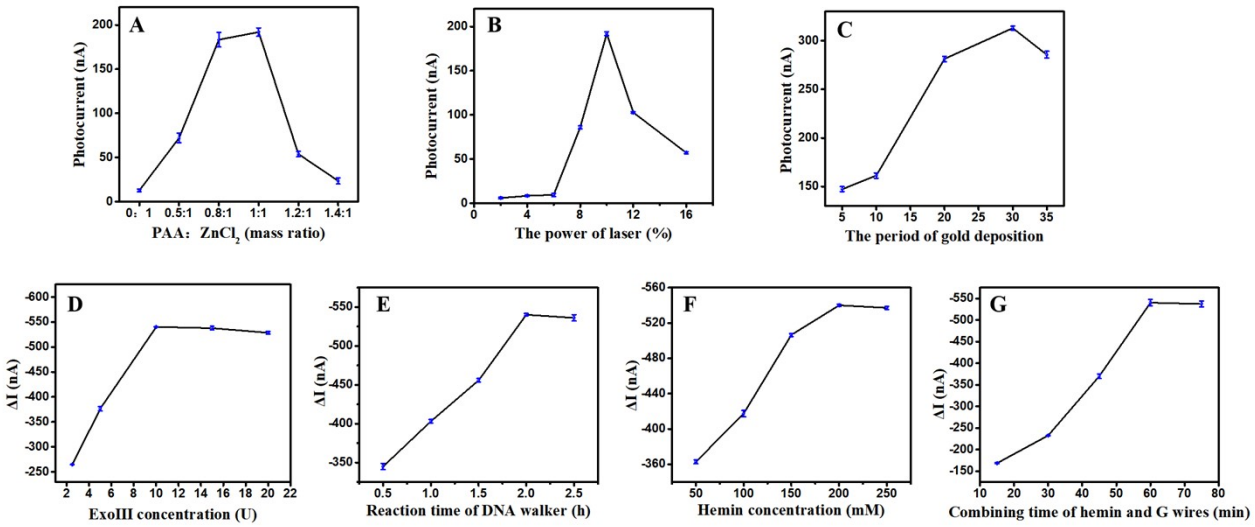

Fig S2. Effects of (A) PAA to $ZnCl_2$ mass ratio, (B) laser power, (C) Au NPs deposition cycle, (D) Exo III concentration, (E) DNA walker reaction time, (F) hemin concentration, and (G) hemin and G wires binding time on photocurrent response of PEC biosensor.

References

1. J. Zhao, C. Zheng, J. Gao, J. Gui, L. Deng, Y. Wang and R. Xu, *Sens. Actuators, B*, 2021, **347,** 130653.

2. X. Liu, H. Cheng, Y. Zhao, Y. Wang and F. Li, *Biosens. Bioelectron.*, 2022, **199**, 113906.

3. P. Hohenberg and W. Kohn, *Phys. Rev.*, 1964, **136**, 864-871.

4. W. Kohn and L. J. Sham, *Phys. Rev.*, 1965, **140**, 1133-1138.

5. G. G. Kresse and J. J., Furthmüller, *Phys. Rev. B*, 1996, **54**, 11169.

6. P. E. Blochl, *Phys. Rev. B*, 1991, **50**, 17953-17979.

7. A. D. Becke, *J. Chem. Phys*., 2014, **140**, 301.

8. C. Adamo and V. Barone, *J. Chem. Phys.*, 1999, **110,** 6158-6170.

9. J. P. Perdew, K. Burke and M. Ernzerhof, *Phys. Rev. Lett.*, 1996, **77**, 3865.

10. S. Grimme, J. Antony, S. Ehrlich and H. Krieg, *J. Chem. Phys.*, 2010, **132**, 154104.

11. H. J. Monkhorst and J. D. Pack, *Phys. Rev. B*, 1976, **13**, 5188-5192.

12. Y. Xu and S. A. A. Martin, *Am. Mineral.*, 2000, **85**, 543-556.

13. F. Weigend and R. Ahlrichs, *Phys. Chem. Chem. Phys.*, 2005, **7**, 3297-3305.